JOURNAL OF MATERIALS SCIENCE **39** (2004) 3641–3646

Thermal stability and optical transition of Er^{3+} in sodium-lead-germanate glasses

ZHONGMIN YANG, SHIQING XU, SHIXUN DAI, JIANHU YANG, LILI HU, ZHONGHONG JIANG
Shanghai Institute of Optics and Fine Mechanics, Chinese Academy of Sciences, Shanghai 201800, People's Republic of China
E-mail: wuhanyangzm@yahoo.com

The thermal stability and spectroscopic properties of Er^{3+}-doped Na_2O-GeO_2-PbO glasses were investigated experimentally. The thermal analysis results show that the thermal stability of the investigated glasses is improved with replacing GeO_2 by PbO. Subsequently, Judd-Ofelt (J-O) approach was applied to the room temperature absorption of Er^{3+} ($4f^{11}$) transitions to determine J-O intensity parameters. The reduced values of Ω_2 with the substitution of PbO for GeO_2 indicate the decrease of covalency of Er—O bonding. The stimulated emission cross section of the $^4I_{13/2} \rightarrow {}^4I_{15/2}$ transition increases as a consequence of the increase of refractive index of glass hosts and the narrowing of fluorescence bandwidth with the increase of PbO. The abnormal large emission cross section and large bandwidth in the Na_2O-$0.8GeO_2$-0.1PbO glass arises from the change of germanium coordination with oxygen.

1. Introduction

Heavy metal oxide (HMO) glasses are becoming an important class of materials for optoelectronics applications because of their high refractive index and low phonon energy [1–5]. The reduced phonon energy increases the quantum efficiency of luminescence from excited states of rare-earth ions and provides the possibility to develop more efficient lasers and fiber optic amplifiers at longer wavelength than available from other oxide glasses [6, 7]. On the other hand, optical integrated circuits are needed to make optical functions in low-loss and low-cost chips. In this case, short active length is needed, and high rare-earth ion doping concentration should be used.

Of HMO glasses, germanate based glasses have potential for optical devices because of their low transmission loss in the mid-infrared region [7–10]. Recently, these glasses have been drawn into optical fibers due to their good mechanical strength, high thermal stability, and better chemical durability [11]. Various modifiers, such as PbO, Bi_2O_3, TeO_2, and TiO_2, can be added into GeO_2 to produce more stable glass. Of these, PbO is a suitable modifier, and glasses containing up to 50 mol% PbO can be obtained [12]. Moreover, lead-germanate based glass systems have been reported as having a high infrared transmittance. In this article, we first investigated the dependence of thermal stability on glass host constitutions and then studied the photoluminescence properties of Er^{3+} in sodium-lead-germanate glass.

2. Experimental

2.1. Glass preparation

The glass samples studied have the following compositions in mol: $0.1Na_2O$-$(0.9 - x)GeO_2$-xPbO, where $x = 0$, 0.1, 0.2, 0.3, 0.4, respectively. They were prepared from reagent grade sodium carbonate (Na_2CO_3), lead oxide (Pb_3O_4), and high purity germanium oxide (GeO_2) (>99.999%). Er^{3+} ions were introduced as Er_2O_3 with 99.99% purity and the doping concentration was presented in Table I. Batches of 20 g were well mixed in appropriate proportions and melted in an alumina crucible in a SiC-resistance electric furnace at temperatures between 1050 and 1350°C for 15 min. The homogenous bubble-free melts were cast on a stainless plate and well annealed in a muffle furnace to reduce the thermal stress of glasses.

The samples were cut using a low-speed diamond saw and polished with 5 μm diamond paste. The two-face polished samples have a plate shape with $20 \times 10 \times 2$ mm for optical measurements.

2.2. Measurements of glass properties

The refractive indexes of the studied glasses were measured using the Brewster angle method. The density of samples was measured by Archimedes' liquid-immersion method on an analytical balance with an accuracy of 0.0001 g. The transition temperature, T_g, and onset crystallization temperature, T_x, were analyzed with differential thermal analyses (DTA) at a heating rate of 10°C/min.

TABLE I Er^{3+} concentration, refractive index and density of $0.1Na_2O$-$(0.9-x)GeO_2$-$xPbO$ glasses

Glass sample	Composition (mol)	Er^{3+} concentration ($\times 10^{20}$ ions/cm^3)	Refractive index (n_d)	Density (g/cm^3)
NG0	$x = 0$	4.752	1.66997	4.152
NG1	$x = 0.1$	4.714	1.72856	4.5889
NG2	$x = 0.2$	4.654	1.77635	4.9931
NG3	$x = 0.3$	4.644	1.84337	5.4437
NG4	$x = 0.4$	4.568	1.91301	5.8087

Absorption spectra of glass samples were recorded with a PERKIN-ELMER-LAMBDA 900UV/VIS/NIR spectrophotometer in the range of 380–1700 nm. Luminescence measurements were performed with a 970 nm diode laser (2W) excitation and detected by a TRIAX550 spectrophotometer controlled by a computer.

All the measurements were taken at room temperature.

3. Results and discussions

3.1. Thermal analysis

The prepared sodium-lead-germanate glasses are clear and transparent for all compositions, with a slight pink color due to the addition of Er_2O_3. In addition, a gradually deeping yellow color can also discerned with increasing PbO content. These glasses exhibit no visual evidence of phase separation, which occurs in many binary glass systems containing PbO [13].

Fig. 1 shows the dependence of T_g, T_x, and $\Delta T = T_x - T_g$ of $0.1Na_2O$-$(0.9-x)GeO_2$-$xPbO$ ($x = 0$, 0.1, 0.2, 0.3, and 0.4) glasses on PbO content. It can be observed that the T_g and T_x monotonically decrease accompanying the increase of PbO, while the difference between T_x and T_g increases. ΔT is frequently used as a rough estimate of the glass formation ability and glass stability [14]. To achieve a large working range of temperature during fiber drawing, it is desirable for a glass host to have ΔT as large as possible. In our cases, a maximum value of ΔT in the glass $0.1Na_2O$-$0.5GeO_2$-$0.4PbO$ indicates that the glass have a good ability resistant to devitrification.

Numerous infrared and Raman spectroscopic studies show that in vitreous GeO_2, GeO_4 tetrahedra construct a three-dimensional random network through sharing the vertex oxygen atoms as do SiO_4 tetrahedra in vitreous SiO_2 [15–17]. As an alkali is added to the germanate another half of an oxygen is added as well. Partial conversion of germanium coordination with oxygen from four (tetrahedral) to six (octahedral) occurs when alkali oxide is increased to ~20 mol%. Recent neutron scattering experiment for PbO-GeO_2 glasses confirmed that the octahedral units exist even at high PbO content, for example, 30 mol% [18]. The co-existence of octahedral and tetrahedral units of germanium may decrease the stability of glass against devitrification. At low PbO (≤20 mol%) content, ΔT increases slightly with increasing PbO and subsequent replacement of GeO_2 by PbO results in a rapid increase of ΔT. This trend is closely related to the content of octahedral units. With the decrease of Ge-O octahedral content the thermal stability of glasses is improved.

3.2. Absorption spectra and Judd-Ofelt analysis

The absorption spectra of the glasses are presented in Fig. 2 where the absorption bands are assigned to transitions from the ground state ($^4I_{15/2}$) to excited states of the Er^{3+} ion. It was observed that the cutoff wavelengths of the studied glass in the near-ultraviolet region are lower than 400 nm and shifted to longer wavelength with increasing PbO.

Judd-Ofelt (J-O) theory is one of the most successful theories in estimating the magnitude of the forced electric dipole transitions of rare-earth ions. In the J-O approach, the line strength for an electric-dipole transition between two J states has been given by [19]

$$S_{\mathrm{calc}}(J \to J') = \sum_{t=2,4,6} \Omega_t \left| \left\langle 4f^N(SL)J \left\| U^{(t)} \right\| 4f^N(S'L')J' \right\rangle \right|^2 \quad (1)$$

where J and J' are the total angular momentum quantum members of the initial and final states, respectively. Ω_2, Ω_4, and Ω_6 are the J-O intensity parameters, and $\langle \| U^{(t)} \| \rangle$ are the doubly reduced matrix elements of rank $t (t = 2, 4, 6)$ between states characterized by the

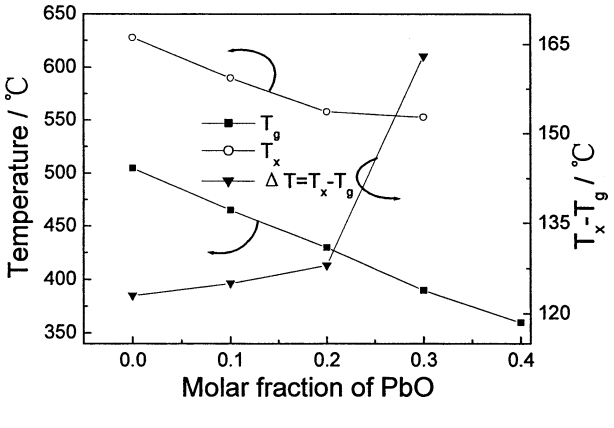

Figure 1 Compositional dependence of T_g, T_x, and ΔT of $0.1Na_2O$-$(0.9-x)GeO_2$-$xPbO$ ($x = 0$, 0.1, 0.2, 0.3, and 0.4) glasses.

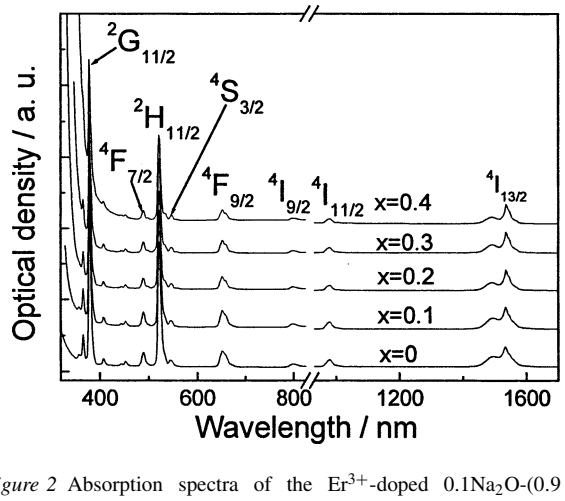

Figure 2 Absorption spectra of the Er^{3+}-doped $0.1Na_2O$-$(0.9-x)GeO_2$-$xPbO$ glasses.

quantum members (S, L and J) and (S', L', and J'). Because the matrix elements are essentially the same from host to host, we used the values calculated by Weber for Er^{3+} in LaF_3 [20].

The measured line strengths, $S_{meas}(J \rightarrow J')$, of an absorption band can be calculated using the experimental values of the integrated absorbance. This relationship is

$$S_{meas}(J \rightarrow J') = \frac{3ch(2J+1)}{3.44\pi^3 l\bar{\lambda}e^2N_0}\left[\frac{9n}{(n^2+2)^2}\right] \times \int OD(\lambda)d\lambda \quad (2)$$

where c is the speed of light, h is Plank's constant, N_0 is the Er^{3+} ion concentration, $\bar{\lambda}$ is the mean wavelength of the specific absorption band, n is the refractive index, 1 is the thickness of the investigated sample, e is the electron charge, OD(λ) is optical density as a function of λ. The J-O intensity parameters Ω_t can be determined by a least-squares fitting of Equation 1. The absorption bands measured are all dominated by electric-dipole transitions except the transition $^4I_{15/2} \rightarrow {}^4I_{13/2}$ for which magnetic-dipole transition is involved. The electric-dipole oscillator strength (S_{ed}) for the $^4I_{15/2} \rightarrow {}^4I_{13/2}$ transition was obtained by subtracting the calculated magnetic-dipole oscillator strength (S_{md}). Based on the J-O intensity parameters, the following properties of glass can be evaluated:

1. The spontaneous emission probability from an initial state $|(S, L)J\rangle$ to a final manifold $|(S', L')J'\rangle$ is

$$A(J \rightarrow J') = \frac{64\pi^4e^2}{3h(2J'+1)\bar{\lambda}^3}\frac{n(n^2+2)^2}{9} \times S_{calc}(J \rightarrow J') \quad (3)$$

2. The fluorescence branching ratio for transitions from an initial state $|(S, L)J\rangle$ to lower levels $|(S', L')J'\rangle$ is

$$\beta(J \rightarrow J') = \frac{A(J \rightarrow J')}{\sum A(J \rightarrow J')} \quad (4)$$

3. The radiative lifetime is given by

$$\tau_{calc} = A_{total}^{-1} \quad (5)$$

4. The radiative quantum efficiency of the $|(S, L)J\rangle$ manifold is defined as

$$\eta = \tau_{meas}/\tau_{calc} \quad (6)$$

where τ_{meas} is the measured fluorescence lifetime.

The calculated J-O intensity parameters for Er^{3+} doped $0.1Na_2O$-$(0.9-x)GeO_2$-$xPbO$ glasses are shown in Table II. It can be seen that the replacement of GeO_2 by PbO results in a monotonic decrease of Ω_2 and Ω_6. Furthermore, the magnitude of Ω_2 is greater than that of Ω_4 and Ω_6 in each case. Previous studies revealed that the Ω_2 parameter is indicative of the amount of the covalency of Er–O bond and is sensitive to the local environments of Er^{3+} ion sites, whereas the Ω_6 parameter is related to the rigidity of host or the overlap integrals of the $4f$ and $5d$ orbits [21, 22]. The decrease of Ω_2 with the substitution of PbO for GeO_2 indicates that there Er–O bonding in high PbO-containing glasses has more ionic nature. For comparison, we list the Ω_t of various glasses in Table III. It is obvious that germanate glass, compared with fluoride glass, has larger Ω_2 and smaller Ω_6, indicating that fluoride glass have more ionic than germanate glasses. Compared with other oxide glasses [23], germanate glasses have medium values of Ω_2 and small Ω_6, which indicates that the viscosity and rigidity of the germanate glasses are larger.

TABLE II J-O intensity parameters for Er^{3+} in $0.1Na_2O$-$(0.9-x)GeO_2$-$xPbO$ glasses with different PbO content x

Glass sample	Ω_2 ($\times10^{-20}$ cm^2)	Ω_4 ($\times10^{-20}$ cm^2)	Ω_6 ($\times10^{-20}$ cm^2)	Rms (%)
NG0	6.87	1.49	0.86	0.52
NG1	5.88	1.50	0.62	3.0
NG2	5.12	1.06	0.4	1.30
NG3	4.48	0.89	0.32	1.30
NG4	3.84	0.71	0.25	0.85

TABLE III J-O intensity parameters of Er^{3+} in various glasses [23]

Glass	Ω_2 ($\times10^{-20}$ cm^2)	Ω_4 ($\times10^{-20}$ cm^2)	Ω_6 ($\times10^{-20}$ cm^2)	Rms[a] (%)
Aluminate	5.60	1.60	0.61	8.1
Silicate	4.23	1.04	0.61	5.4
Phosphate	6.65	1.52	1.11	4.8
Fluoride	2.91	1.27	1.11	3.4
Bismuth-base glass	4.73	1.31	0.94	1.9

[a]Rms $= [\sum(f_{calc} - f_{meas})^2/\sum f_{meas}^2]^{1/2}$ where f_{calc} and f_{meas} are the calculated and measured oscillator strengths, respectively.

3.3. Fluorescence spectra and emission cross section

Fig. 3 shows the normalized emission spectra of the $^4I_{13/2} \rightarrow {}^4I_{15/2}$ transition of Er^{3+} in $0.1Na_2O$-$(0.9-x)GeO_2$-$xPbO$(x = 0, 0.1, 0.2, 0.3, and 0.4) glasses excited at 970 nm. With replacement of GeO_2 by PbO,

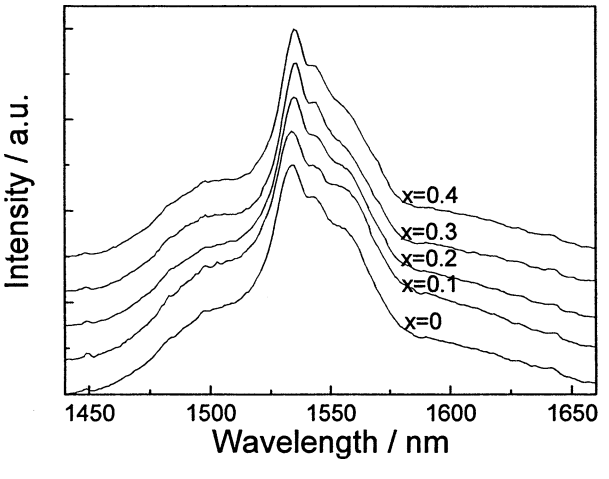

Figure 3 Normalized emission spectra of the $^4I_{13/2} \rightarrow {}^4I_{15/2}$ transition of Er^{3+} in $0.1Na_2O$-$(0.9-x)$ GeO_2-$xPbO$ (x = 0, 0.1, 0.2, 0.3, and 0.4) glasses excited at 970 nm.

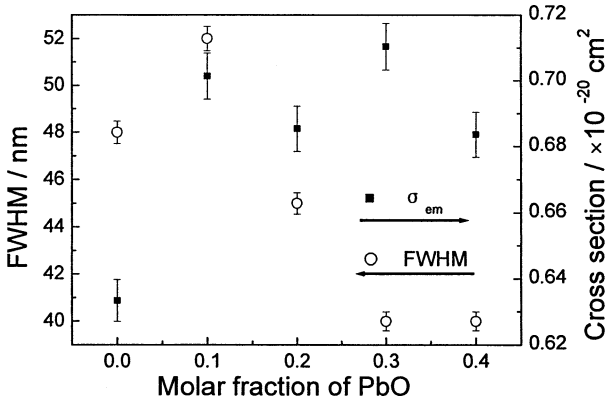

Figure 4 Compositional dependence of FWHM and stimulated emission cross section of the $^4I_{13/2} \rightarrow {}^4I_{15/2}$ transition of Er^{3+} in $0.1Na_2O$-$(0.9-x)GeO_2$-$xPbO$ ($x = 0$, 0.1, 0.2, 0.3, and 0.4) glasses.

the peak wavelength of fluorescence band is slightly shifted to longer wavelength direction. In different glass host the full width at half maximum (FWHM) of fluorescence spectrum is often used as a semiquantitative indication to evaluate the bandwidth. Furthermore, the bandwidth is a measure of the overall extent of the Stark splitting of J manifolds and is inhomogeneous due to the site-to-site variations in the local field [24]. Fig. 4 shows the dependence of FWHM of the $^4I_{13/2} \rightarrow {}^4I_{15/2}$ transition of Er^{3+} in the investigated glasses. It is obviously noted that the FWHM increases first and then decreases monotonically. These results reveal that the ligand field around Er^{3+} is changed with the increase of PbO. As mentioned above, the non-bridging oxygen atoms generated from the substitution of PbO for GeO_2 tend to incorporate with Er^{3+}. The decrease of covalency between Er and O reduces the extent of Stark splitting of the $^4I_{15/2}$ and $^4I_{13/2}$ manifolds, resulting in a decrease of FWHM. In addition, according to J-O theory, the electric-dipole transition is a main contribution to the fluorescence bandwidth because the magnetic-dipole transition is independent of the glass host and determined only by quantum numbers. The S_{ed} of the $^4I_{13/2} \rightarrow {}^4I_{15/2}$ transition of Er^{3+} can be expressed by

$$S_{ed}\left[{}^4I_{13/2} \rightarrow {}^4I_{15/2}\right] = 0.0188\Omega_2 + 0.1176\Omega_4 + 1.4617\Omega_6 \quad (7)$$

where the three coefficients of Ω_{ts} are the reduced matrix elements of the unit tensor operators provided in Ref. [20]. Obviously, S_{ed} is mainly determined by the Ω_6 parameter because of the small values of the first two coefficients. Table IV presents the calculated S_{ed} and S_{md} of the $^4I_{13/2} \rightarrow {}^4I_{15/2}$ transition. It can be seen that the values of S_{ed} decrease with the increase of PbO.

As for the increase of FWHM for the NG1 glass, it may be due to the "germanate anomaly effect". When modifier oxides are added up to ~20 mol%, the site-to-site variations in the local field around Er^{3+} is remarkable due to the existence of a large amount of 6-coordinated Ge units, resulting in the inhomogeneous broadening of fluorescence spectrum.

According to the McCumber theory [25], the stimulated emission cross section (σ_e) of the $^4I_{13/2} \rightarrow {}^4I_{15/2}$ transition of Er^{3+} can be calculated from the absorption cross section (σ_a), which is related by

$$\sigma_e(\lambda) = \sigma_a(\lambda)\exp[(\varepsilon - h\nu)/kT] \quad (8)$$

where k is the Boltzmann constant, and ε is the free energy required to excite one Er^{3+} from the ground state to the $^4I_{15/2}$ state at temperature T. σ_a and ε can be calculated from the absorption spectra. Fig. 4 shows the dependence of the stimulated emission cross section on the PbO content. Obviously, the glasses containing PbO have large stimulated emission cross section. This is due to the large density and small FWHM in PbO-containing glasses. Previous research showed that the peak emission cross section was proportional to the refractive index of glass host ($\sigma \propto (n^2+2)^2/n$) and inversely proportional to the fluorescence linewidth [26]. However, the fluctuant distribution of σ_e in our experiments, as shown in Fig. 4, demonstrates that the emission cross section is not a monotonic relation with refractive index and fluorescence linewidth.

Table V shows the peak emission cross section (σ_e^{Peak}) and FWHM of Er^{3+} in various glasses. It is clear that the σ_e^{Peak} of NG1 glass is larger than that of phosphate and silicate glasses and is comparable to that of tellurite and bismuth-base glasses. The FWHM is also larger than that of silicate and phosphate glasses, but smaller than that of tellurite and bismuth-base glasses. The bandwidth properties of optical amplifiers can be evaluated from the product of FWHM and σ_e^{Peak}. The bigger the product, the better the properties [23]. In our cases the product of FWHM and σ_e^{Peak} of NG1 glass is bigger than that of silicate and phosphate glasses, but smaller than that of tellurite and bismuth-base glasses.

3.4. Effect of PbO on the $^4I_{13/2}$ lifetime

Fig. 5 shows the compositional dependence of the lifetime and quantum efficiency of the $^4I_{13/2}$ level of Er^{3+} in $0.1Na_2O$-$(0.9-x)GeO_2$-$xPbO$ ($x = 0$, 0.1, 0.2, 0.3,

TABLE IV Calculated line strength of the $^4I_{13/2} \rightarrow {}^4I_{15/2}$ transition and lifetimes of Er^{3+} in $0.1Na_2O$-$(0.9-x)GeO_2$-$xPbO$ glasses

Glass sample	Average frequency (cm^{-1})	S_{ed}	S_{md}	τ_{calc} (ms)
NG0	6 521	1.5614	0.7227	7.63
NG1	6 515	1.1932	0.7227	8.10
NG2	6 515	0.8056	0.7227	9.22
NG3	6 508	0.6566	0.7227	9.03
NG4	6 508	0.5211	0.7227	8.85

TABLE V σ_e^{Peak} and FWHM of Er^{3+} in various glasses [23]

Glass sample	n_d	σ_e^{Peak} (10^{21} cm^2)	FWHM (nm)	σ_e^{Peak} × FWHM
NG1	1.667	7.0	52	364
Silicate	1.585	5.5	40	220
Phosphate	1.569	6.4	37	236.8
Tellurite	2.019	7.5	65	487.5
Bismuth-base glass	1.945	7.0	79	554

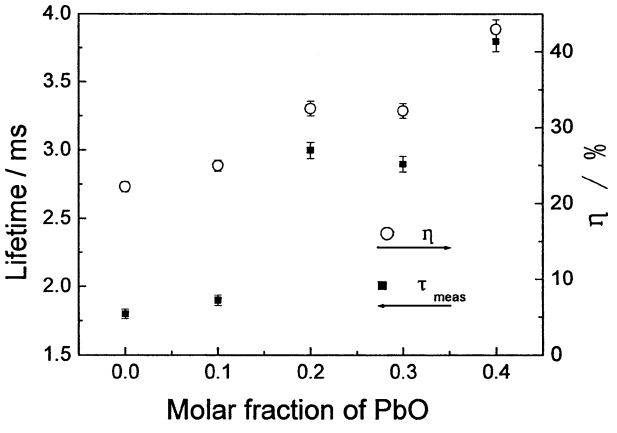

Figure 5 Compositional dependence of lifetime and quantum efficiency of the $^4I_{13/2}$ level in $0.1Na_2O$-$(0.9-x)GeO_2$-$xPbO$ ($x = 0$, 0.1, 0.2, 0.3, and 0.4) glasses.

and 0.4) glasses. It can be seen that the lifetime of the $^4I_{13/2}$ level and the quantum efficiency (η) of the $^4I_{13/2} \rightarrow {}^4I_{15/2}$ transition increase with the increase of PbO. The lifetime of $^4I_{13/2}$ level of Er^{3+} is influenced by the maximum phonon energy of the glass host. With the addition of PbO the maximum vibration frequency of glass host is shifted from ~900 to 800 cm^{-1} [27, 28]. The reduced maximum phonon energy decreases the non-radiative decay rate, resulting in the increase of the lifetime and quantum efficiency. Table IV lists the lifetime of the $^4I_{13/2}$ state of Er^{3+} calculated by J-O theory. It can be observed that the lifetimes of the $^4I_{13/2}$ level first increase and then decrease with the replacement of GeO_2 by PbO. According to J-O theory, the lifetime of the $^4I_{13/2}$ level is inversely proportional to the refractive index and the line strength of electric-dipole transition of the $^4I_{13/2} \rightarrow {}^4I_{15/2}$ transition. With the increase of PbO the refractive index of glass host increases, whereas the line strength of the electric-dipole transition decreases due to the monotonic decrease of Ω_6. As a result, the calculated lifetimes first increase and then decrease accompanying the replacement of GeO_2 by PbO. The low lifetime and quantum efficiency are also observed in Fig. 5. These are due to the quenching effect from free OH^-. It is found in our experiments that the germanate glasses with high GeO_2 content have poor resistance to moisture atmosphere. The strong stretching vibration of OH^- at 3600 cm^{-1} (2.79 μm) makes OH groups the fluorescence-quenching centers [29]. Only two OH^- vibrational quanta are required to bridge the energy gap between the $^4I_{13/2}$ and $^4I_{15/2}$ levels. Therefore nonradiative decay occurs under the excitation of 970 nm laser. In addition, the high doping concentration of Er^{3+} is another reason to reduce the excited state lifetime and quantum efficiency due to the cross relaxation between rare-earth ions [30].

4. Conclusions

The thermal analysis of Er^{3+}-doped $0.1Na_2O$-$(0.9-x)GeO_2$-$xPbO$ ($x = 0$, 0.1, 0.2, 0.3, and 0.4) glasses was performed and the results show that the thermal stability of glasses is improved with the replacement of GeO_2 by PbO. No crystallization band appears in the Na_2O-$0.5GeO_2$-0.4PbO glass during the DTA measurement. Subsequently, the absorption spectra were measured and analyzed. For the $^4I_{15/2} \rightarrow {}^4I_{13/2}$ transition of Er^{3+}, with the increase of PbO from 0 to 40 mol%, the absorption peak wavelength shifts from 1533.5 to 1536.5 nm. J-O analyses show that the covalency of Er—O bonding decreases with the replacement of GeO_2 by PbO.

The luminescence spectra of Er^{3+} in $0.1Na_2O$-$(0.9-x)GeO_2$-$xPbO$ ($x = 0$, 0.1, 0.2, 0.3, and 0.4) glasses were measured. The stimulated emission cross section of the $^4I_{13/2} \rightarrow {}^4I_{15/2}$ transition increases as a consequence of the increase of refractive index of glass hosts and the narrowing of fluorescence bandwidth with the increase of PbO. As for the relatively larger stimulated emission cross section and FWHM in NG1 glass, these arise from the germanate anormaly effect.

Both the measured lifetime and quantum efficiency of the $^4I_{13/2} \rightarrow {}^4I_{15/2}$ transition increase with the increase of PbO content. The relatively low lifetime and quantum efficiency result from the quenching effect from OH^- group and high doping concentration of rare-earth ions.

Acknowledgement

This work is sponsored by the National Natural Science Foundations of China (No. 60307004 and 60207006) and the Project of Optical Science and Technology of Shanghai (No. 022261046).

References

1. Y. G. CHOI, J. HEO and V. A. CHERNOV, *J. Non-Cryst. Solids* **221** (1997) 199.
2. A. A. KHARLAMOV, R. M. ALMEIDA and J. HEO, *ibid.* **202** (1996) 233.
3. Y. G. CHOI and J. HEO, *ibid.* **217** (1997) 199.
4. Y. B. SHIN, H. T. LIM, Y. G. CHOI and J. HEO, *J. Amer. Ceram. Soc.* **83** (2000) 787.
5. S. SIMON, I. ARDELEAN and S. FILIP, *Solid State Commun.* **116** (2000) 83.
6. R. BALDA, J. FERNANDEZ, M. SANZ *et al.*, *Phys. Rev.* B **61** (2000) 3384.
7. A. S. OLIVEIRA, M. T. ARAUJO, A. S. GOUVEIA-NETO *et al.*, *J. Appl. Phys.* **83** (1998) 604.
8. J. PORQUE, S. JIANG, B. HWANG *et al.*, *SPIE* **3942** (2000) 60.
9. D. R. MACFARLANE, P. J. NEWMAN, R. PLATHE *et al.*, *ibid.* **3849** (1999) 94.
10. Z. PAN AND S. H. MORGAN, *J. Lumin.* **75** (1997) 301.
11. J. WANG, J. R. LINCOLN, W. S. BROCKLESBY *et al.*, *J. Appl. Phys.* **73** (1993) 8066.
12. D. LEZAL, J. PEDLIKOVA and J. HORAK, *J. Non-Cryst. Solids* **196** (1996) 178.
13. J. E. SHELBY, *J. Amer. Ceram. Soc.* **66** (1983) 414.
14. J. H. YANG, S. X. DAI and Y. F. ZHOU, *J. Appl. Phys.* **93** (2003) 1.
15. E. I. KAMITSOS, Y. D. YIANNOPOULOS, C. P. VARSAMIS and H. JAIN, *J. Non-Cryst. Solids* **222** (1997) 59.
16. H. J. WEBER, *ibid.* **243** (1999) 220.
17. H. J. WEBER and M. HASELHOFF, *ibid.* **232–234** (1998) 708.
18. N. UMESAKI, T. M. BRUNIER and A. C. WRIGHT, *Physica* B **213/214** (1995) 490.
19. M. J. WEBER, *Phys. Rev.* **171** (1968) 283.
20. *Idem., ibid.* **157** (1967) 262.
21. A. R. DEVI and C. K. JAYASANKAR, *J. Non-Cryst. Solids* **197** (1996) 111.

22. J. HEO, Y. B. SHIN and J. N. JANG, *Appl. Opt.* **34** (1995) 4284.
23. J. YANG, S. DAI, S. XU *et al.*,*J. Opt. Soc. Amer.* B **20** (2003) 810.
24. R. R. JACOBS and M. J. WEBER, *IEEE J. Quantum Electron* **QE-12** (1976) 102.
25. D. E. MCCUMBER, *Phys. Rev.* A **134** (1964) A 299.
26. J. S. WANG, E. M. VOGEL and E. SNITZER, *Opt. Mater.* **3** (1994) 187.
27. G. S. HENDERSON and M. E. FLEET, *J. Non-Cryst. Solids* **134** (1991) 259.
28. V. N. SIGAEV, I. GREGORA and P. PERNICE, *ibid.* **279** (2001) 136.
29. Y. G. CHOI and J. HEO, *Phys. Chem. Glasses* **39** (1998) 311.
30. E. MAURICE, G. MONNOM, B. DUSSARDIER and D. B. OSTROWSKY, *J. Opt. Soc. Amer.* B **13** (1996) 693.

Received 26 June 2003
and accepted 3 February 2004